Supporting Information

Giant Zn_{14} Molecular Building Block in Hydrogen-bonded Network with Permanent Porosity for Gas Uptake

Suvendu Sekhar Mondal,[†] Asamanjoy Bhunia,[‡] Alexandra Kelling,[†] Uwe Schilde,[†] Christoph Janiak,*[,‡] and Hans-Jürgen Holdt*[,†]

[†]Institut für Chemie, Anorganische Chemie, Universität Potsdam, Karl-Liebknecht-Straße 24-25, 14476 Potsdam, Germany

[‡]Institut für Anorganische Chemie und Strukturchemie, Heinrich-Heine-Universität, Düsseldorf Universitätsstr. 1, 40225 Düsseldorf, Germany

CONTENTS

1 General Remarks

All reagents and solvents were used as purchased from commercial suppliers (Sigma-Aldrich, Fluka, Alfa Aesar, and others) without further purification, if not stated otherwise. Elemental analysis (C, H, N) was performed on Elementar Vario EL elemental analyzer.

Scanning Electron Micrographs (SEM) image of **1** was taken by Phenom from FEICO.

The linker precursor 4,5-dicyano-2-methoxyimidazole (L1) was synthesized following a published procedure.[1]

2 Experimental Details

Synthesis of $[Zn_{14}(L2)_{12}(O)(OH)_2(H_2O)_4]$ $(DMF)_{18}$ (**1**)

In a sealed tube (Type A, company: Ace) 0.10 g (0.76 mmol) of 4,5-dicyano-2-methoxyimidazole (L1) and $Zn(NO_3)_2 \cdot 4H_2O$ (0.17 g, 0.76 mmol) were dissolved in DMF (6 mL). The sealed tube was closed and the mixture was heated at 135 °C for 6 days and was then allowed to cool down to room temperature with 5 °C per hour. Yellow prismatic crystals are formed (~40 wt%) together with a powder material which was identified as the known IFP-7 (Scheme S1, IFP = Imidazolate Framework Potsdam).[2] We optimized the synthetic condition for better yield and X-ray quality crystals. In a modified synthetic procedure the reaction was run for 6 days at 135 °C, instead of 36 h at 130 °C. The yellow crystals were separated by a sieving technique, wherein the crystals were trapped by a mesh (mesh size: 125 µm) while the powder material (IFP-7) filtered through it.[3] The fine crystalline product was washed with DMF and EtOH and dried in air. Yield: 0.067 g (~40 %) based on L1; ^{13}C CP-MAS NMR: δ =167.1, 164.7, 138.8, 127.7 ppm; elemental analysis: $[Zn_{14}(L2)_{12}(O)(OH)_2(H_2O)_4]\cdot(DMF)_{18}$ = $C_{114}H_{184}N_{66}O_{61}Zn_{14}$; Calcd., C 31.33, H 4.24, N 21.15, Found: C 31.57, H 3.82, N 20.69; IR (KBr pellet): ν_{max} = 3440 (m), 3355 (m), 3205 (m), 1658 (vs), 1548 (s), 1436 (s), 1280 (m), 1101 (m), 734 cm^{-1} (m).

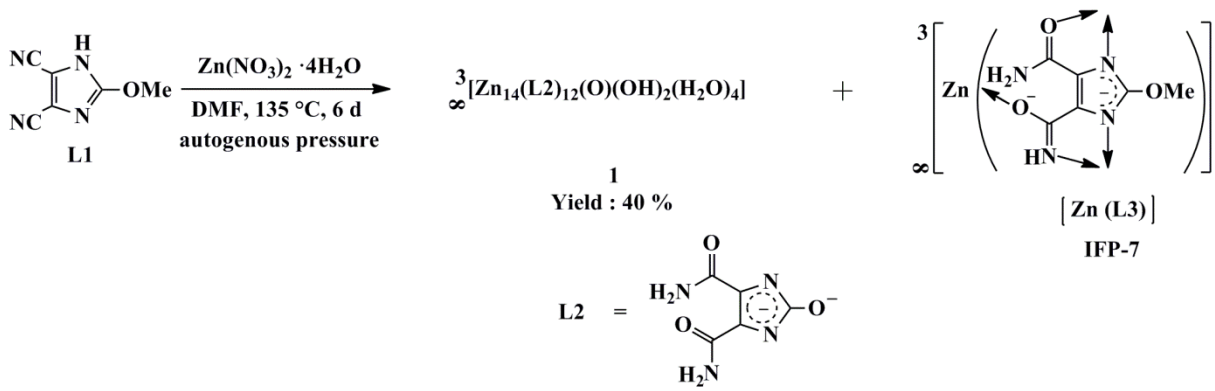

Scheme S1. Syntheses of frameworks **1** and IFP-7.

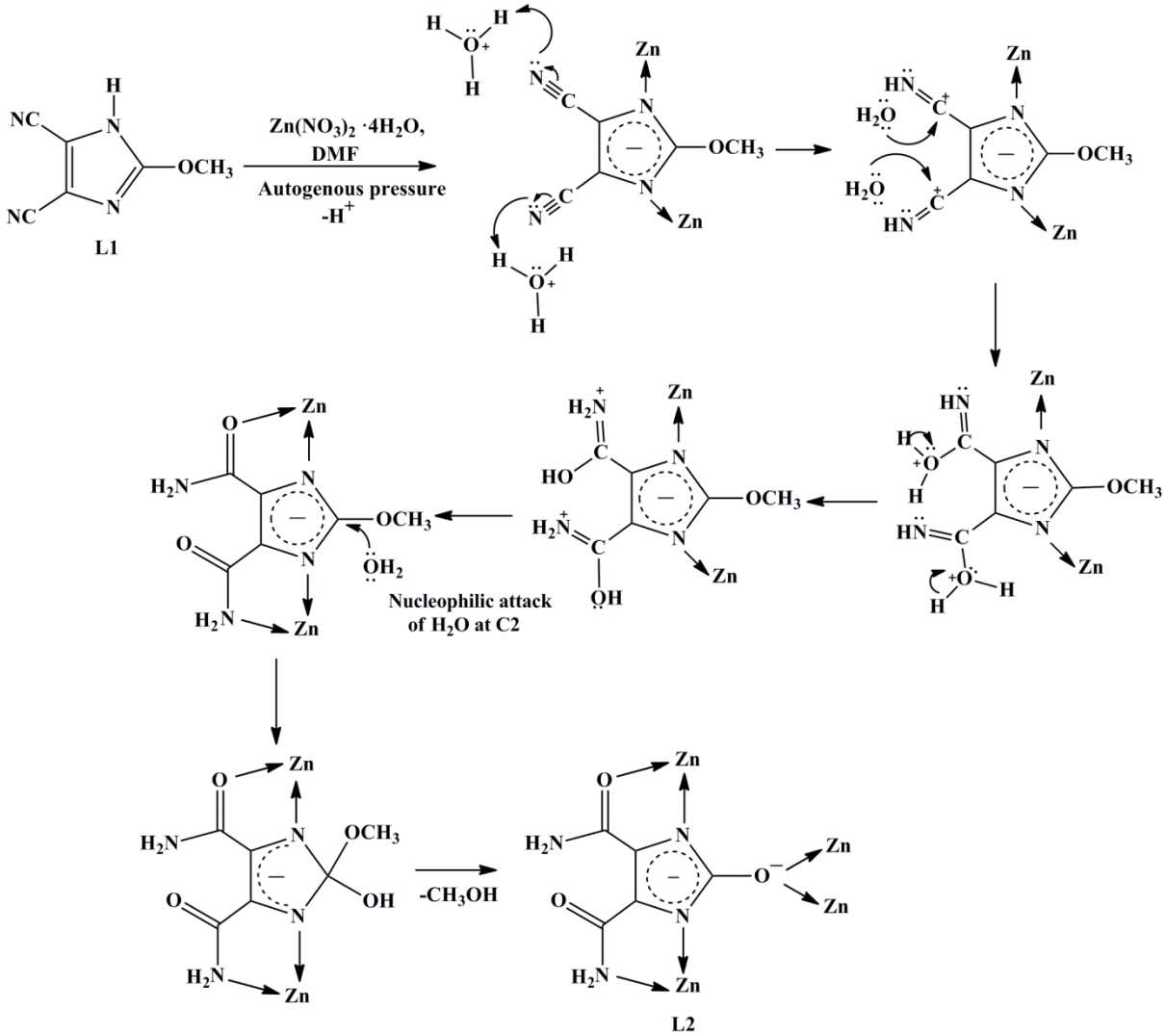

Scheme S2. Proposed *in-situ* linker (L2) generation under solvothermal condition.

3 SEM image

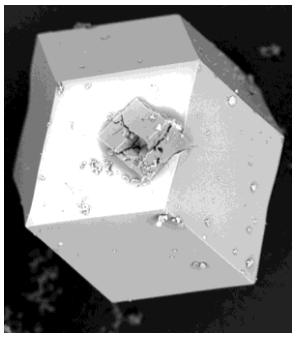

50 μm

Figure S1. Scanning electron micrograph of **1**.

4 IR spectra

IR spectra were recorded on FT-IR Nexus from Thermo Nicolet in the region of 4000 – 400 cm^{-1} using KBr pellets.

A)

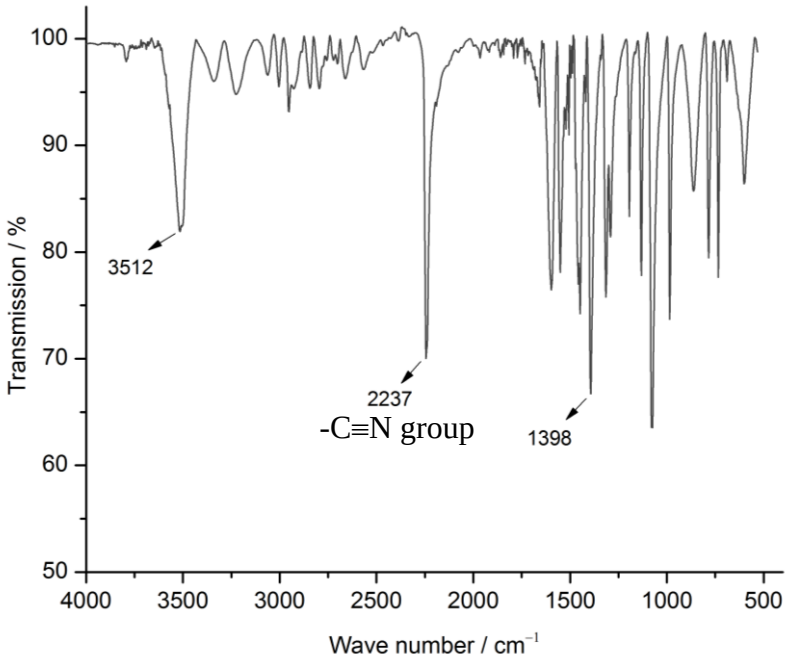

B)

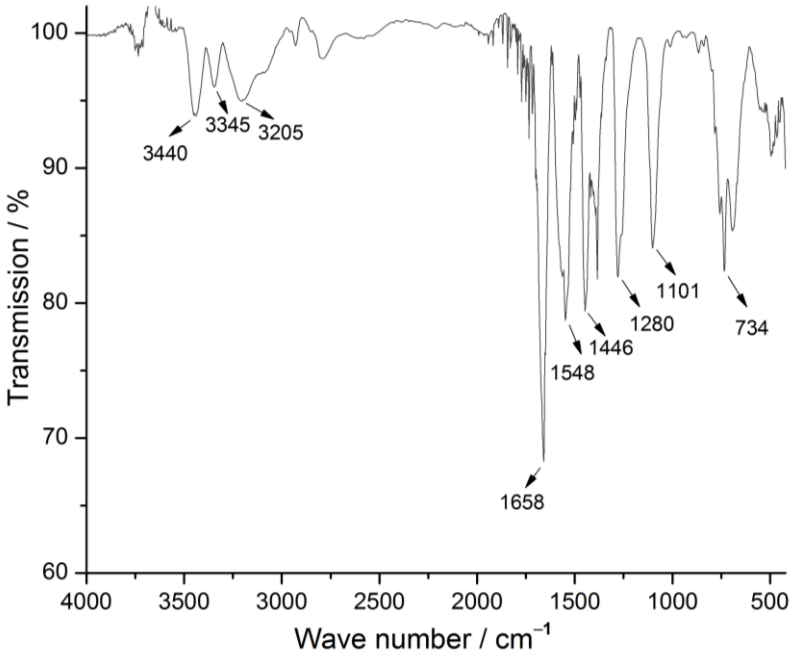

Figure S2. IR-spectra of: **A**) 4,5-dicyano-2-methoxyimidazole (L1); **B**) **1** as-synthesized.

5 NMR Spectroscopy

^{1}H Magic Angle Spinning (MAS) NMR and ^{13}C{^{1}H} Cross Polarization (CP) MAS NMR spectra of as-synthesized 1

^{1}H and ^{13}C Cross Polarization experiments with Magic Angle Sample Spinning (^{13}C CPMAS NMR) were performed on a Bruker Avance 600 spectrometer (Bruker Biospin GmbH, Rheinstetten, Germany, B_0 = 14.1 T) operating at a frequency of 150.9 MHz using a double resonant 4 mm MAS (magic angle sample spinning) probe. The spinning frequency was 12.5 kHz. For CP, a ramped (50 % ramp) lock field was used on the ^{1}H channel with a CP contact time of 2 ms, a recycle delay of 3 s and 512 scans. The 90° ^{1}H pulse length was 3.3 µs. High power TPPM decoupling was applied (B_1 = 80 kHz). The ^{13}C chemical shifts are referenced using the glycine carboxyl group signal (δ(^{13}C) = 176.4 ppm).

^{13}C CP-MAS NMR spectrum is a good evidence of the *in situ* functionalization of cyano groups, as specifically around 165 ppm two peaks appeared for the carbon atoms of the two different amide groups (Figure S3).

A)

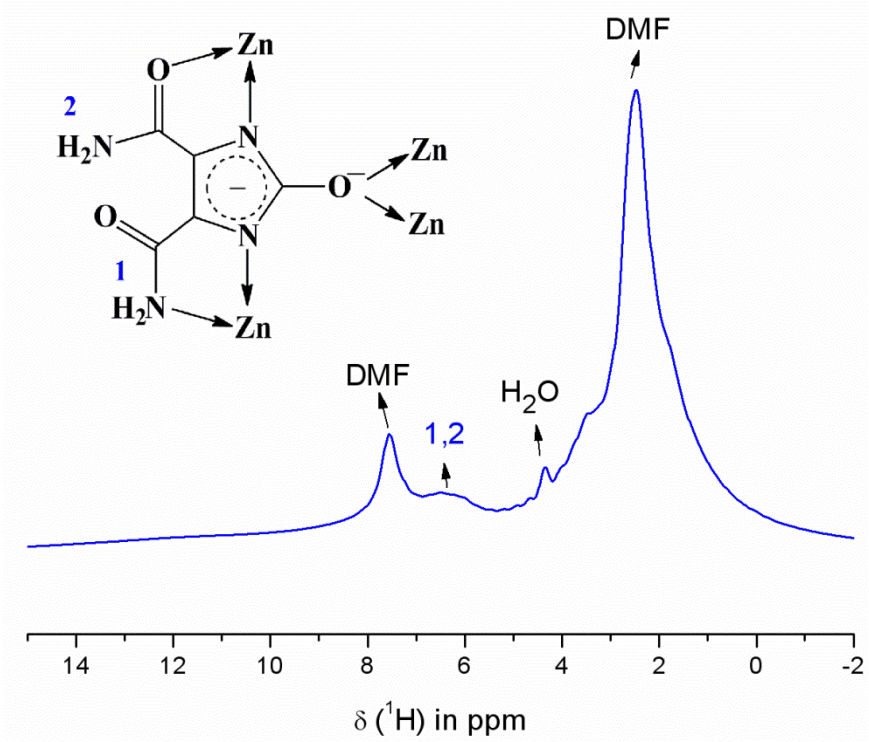

B)

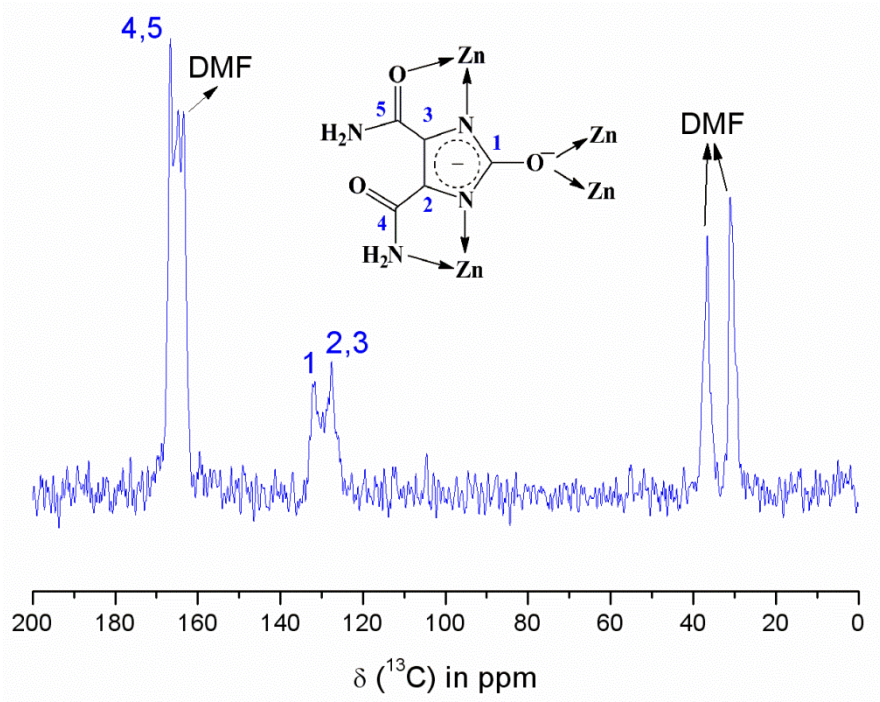

Figure S3. ^{1}H- (**A**) and ^{13}C- (**B**) CPMAS NMR spectra of as-synthesized **1**.

Liquid-phase ^{13}C NMR spectroscopy of activated 1

NMR spectra were recorded with a Bruker Avance 300 spectrometer. Resonances for NMR spectra are reported relative to Me_4Si (δ = 0.0 ppm) and calibrated based on the solvent signal for ^{1}H and ^{13}C.

Liquid-phase ^{13}C NMR spectroscopy of activated **1** sample (26 mg) was digested in 0.5 mL [D_6] DMSO and 0.1 mL DCl (20%)/D_2O.

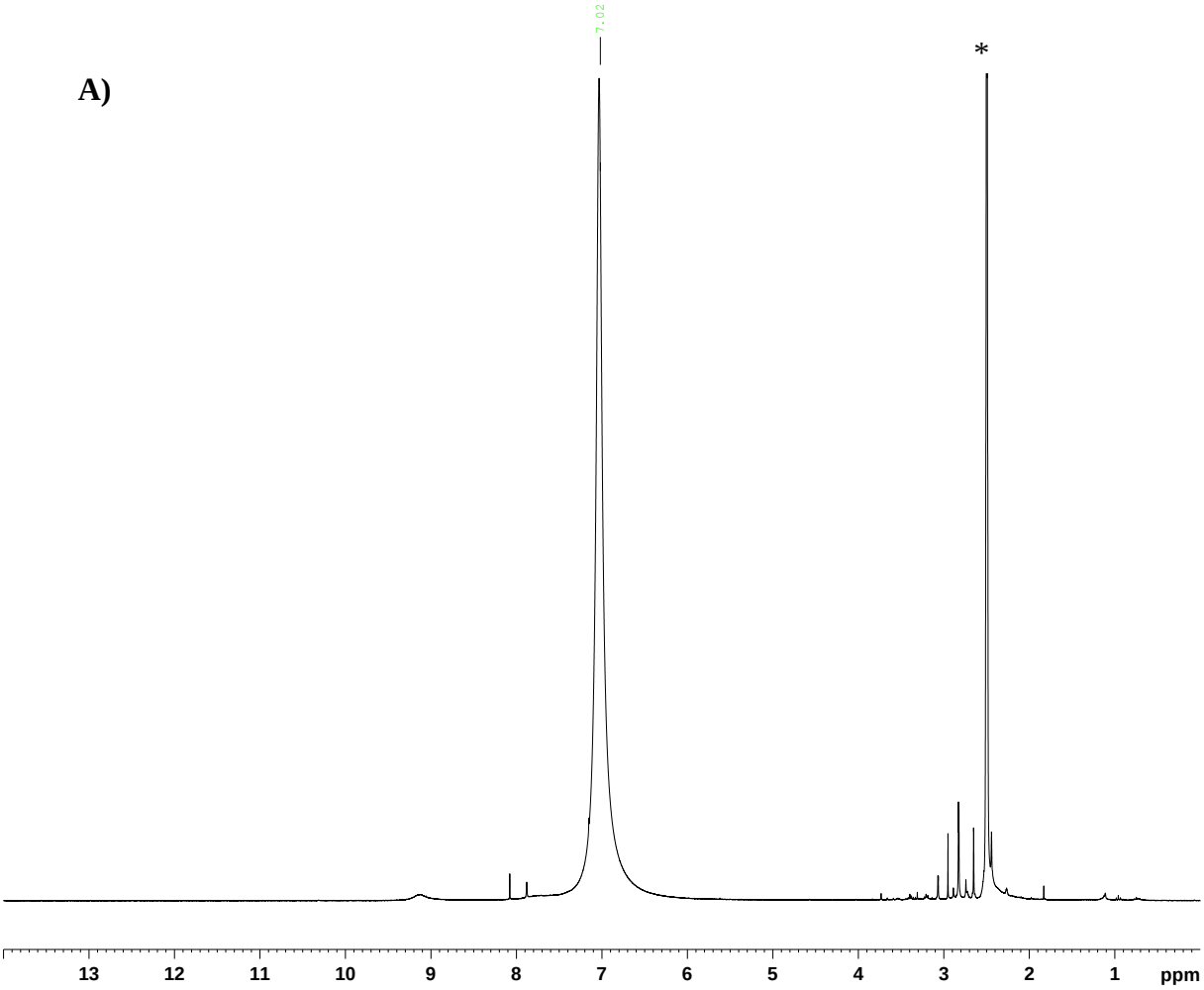

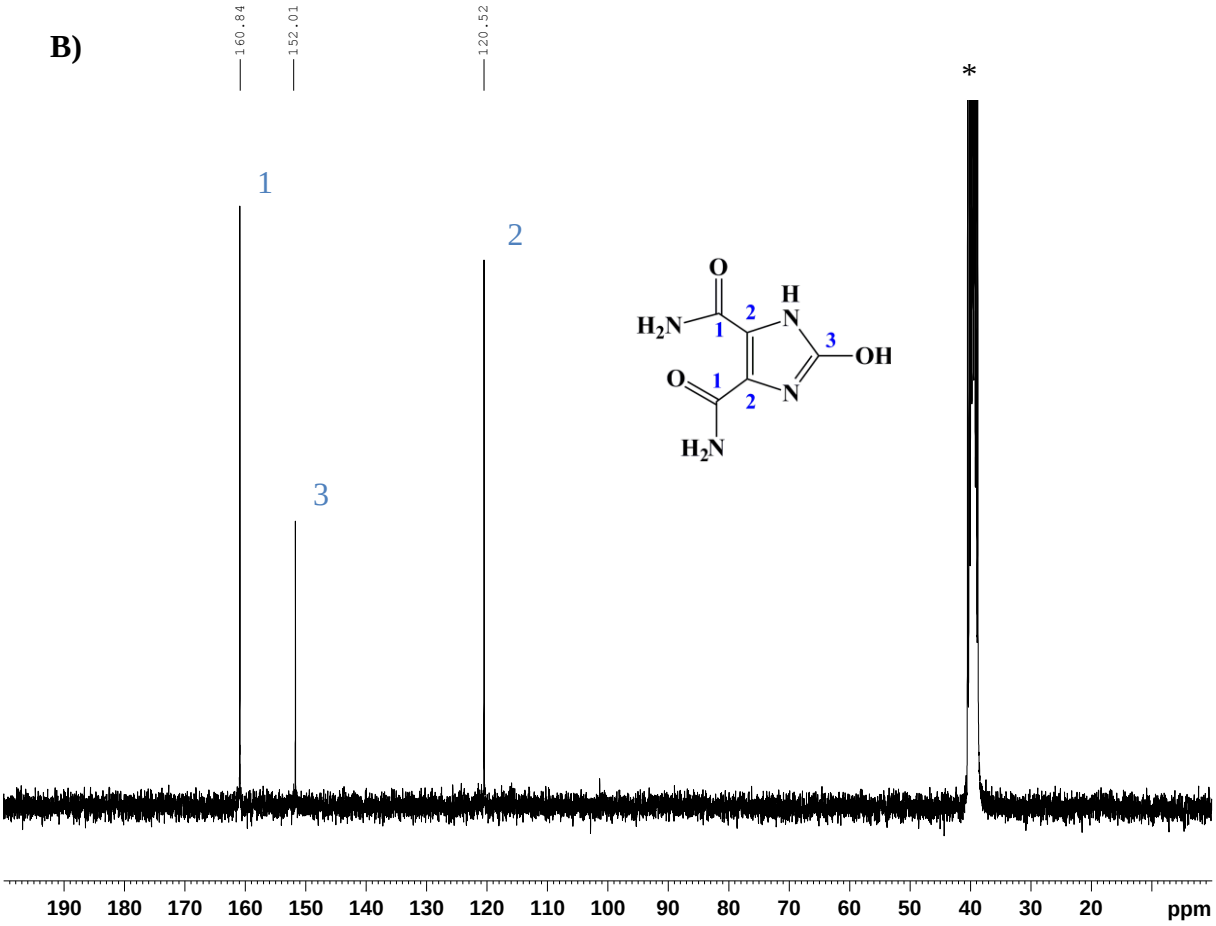

Figure S4. ^{1}H- (**A**) ^{13}C- (**B**) NMR spectra of a digested activated sample **1** in 0.1 mL DCl (20%)/D_2O and 0.5 mL [D_6] DMSO. Solvent signals ([D_6] DMSO) are marked with an asterisk (*). At ^{1}H NMR spectra 2.6–3.0 ppm, weak triplet peaks are observed due to slow HDO intermolecular rate of exchange.[4]

Activated sample did not show any peaks, related to DMF at around 31, 36 and 162 ppm**.**

Digested sample of activated **1** in DMSO-d_6 and DCl/D_2O, there is no coordination to zinc. Moreover, olate group and imidazolate can be protonated. That could be a nice comparison with solid state NMR spectra (deprotonated and coordinated state).

6 Powder X-ray-diffraction patterns

Powder X-ray diffraction (PXRD) patterns were measured on a Siemens diffractometer D5005 in Bragg-Brentano reflection geometry. The diffractometer was equipped with a copper tube, a scintillation counter, automatic incident- and diffracted-beam soller slits and a graphite secondary monochromator. The generator was set to 40 kV and 40 mA. All measurements were performed with sample rotation. Data were collected digitally from 3° to 70° 2θ using a step size of 0.02° 2θ and a count time of 4 seconds per step. The simulated

powder pattern for **1** was calculated using single-crystal X-ray diffraction data and processed by the free Mercury v1.4.2 program provided by the Cambridge Crystallographic Data Centre.

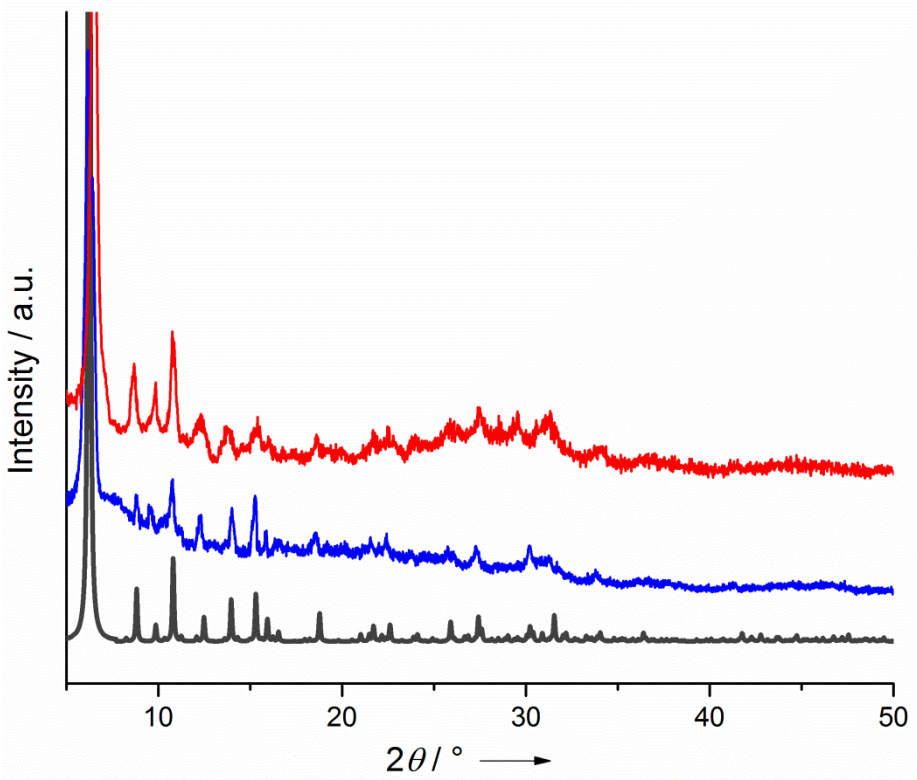

Figure S5. Powder X-ray diffraction patterns of **1** (Color: gray = simulated; blue = as-synthesized, red = activated).

7 Single crystal X-ray structure determination

The crystal was embedded in perfluoropolyalkylether oil and mounted on a glass fibre. Intensity data were collected at 210 K using a STOE Imaging Plate Diffraction System IPDS-2 with graphite monochromatized $Mo_{K\alpha}$ radiation (λ = 0.71073 Å) at 50 kV and 40 mA (180 frames, $\Delta\omega$=1°, exposure time per frame: 1 min). The data were corrected by a numerical absorption correction using the program X-Area (Stoe, 2004) as well as for Lorentz and polarisation effects. The structure was resolved with direct methods using SHELXS-97[5] and refined with full-matrix least-squares on F^2 using the program SHELXL-2013[6] (Sheldrick, 1997). All non-hydrogen atoms were refined anisotropically.

The amide moieties show a high degree of vibrational motion, and attempts to model this behaviour to get better displacement parameters were not fully successful. The hydrogen atoms could not be located from the difference Fourier map and their positions had to be calculated using the AutoCN and HSite options of the Program TOPOS.[7] All hydrogen atoms were involved in the refinement, but their coordinates and temperature factors were fixed.

Therefore the hydrogen bonds can only be characterized by approximate donor-acceptor distances. Residual electron density (2.96 $e^{-}\cdot Å^3$) was found at a threefold axis which could not be assigned to an atom, because the distances to the next oxygen atoms are only 1.8 Å. Even though the data collections were repeated with three other crystals these shortcomings could not rectify. The unit cell contains channels filled with disordered solvent molecules. In spite of several attempts, no chemically reasonable solution could be received for the solvent species in the channels of the crystal material. Very high displacement parameters, high estimates and partial occupancy due to the disorder make it impossible to determine accurate atomic positions for these molecules. Therefore the contribution of the disordered solvent species was subtracted from the structure factor calculations by the SQUEEZE instruction of PLATON. SQUEEZE calculated a solvent-accessible void volume in the unit cell of 34081 $Å^3$ (53 % of the total cell volume), corresponding to 11657 electrons (residual electron density after the last refinement cycle) per unit cell.[8] This number agrees with three molecules of dimethylformamide (3x40x96=11520). The deposited atom data (*cif*) reflect only the refined cell content.

Table S1. Crystal Data, Details of Intensity Measurements, and Structure Refinement for $[Zn_{14}(L2)_{12}(O)(OH)_2(H_2O)_4]$ $(DMF)_{18}$ (= **1**).

Chemical formula, asymmetric unit	$C_{10}H_{9.67}N_8O_{7.17}Zn_{2.33}$
Formula mass	515.80
Crystal system	cubic
Space group	$I\,a\,\bar{3}\,d$ (No 230)
$a = b = c$/ Å	40.1873(12)
$\alpha = \beta = \gamma$ / °	90
Unit cell volume / $Å^3$	64903(6)
Temperature / K	210(2)
Crystal size / mm	0.50 x 0.45 x 0.40
Z	96
Density (calculated) / $g \cdot cm^{-3}$	1.25
Radiation type	MoKα
μ / mm^{-1}	2.10
Theta range / °	1.24-25.00
Index ranges	$-23 \leq h \leq 46$
	$-37 \leq k \leq 47$
	$-47 \leq l \leq 31$
Reflections collected	31851
Independent reflections	4761
R_{int}	0.0653
R_1 / wR_2 [$I > 2\sigma(I)$]	0.0586 / 0.1540
R_1 / wR_2 (all data)	0.0870 / 0.1652
Goodness of fit on F^2	0.861
Max. diff. peak and hole / $e \cdot Å^3$	2.86 / -0.89

Details of structural description:

The asymmetric unit contains three different zinc centres (Zn1, Zn2, Zn3), two imidazolate-4,5-diamide-2-olate ligands (L2) and moreover O^{2-}, OH^- and H_2O. The MBB consists of 14 zinc atoms (six Zn1, six Zn2, two Zn3) and twelve L2 ligands, one O^{2-}(O1), two OH^- (O4) anions and four H_2O (O4) molecules (Figure S6a). The oxide ion (O1) is located in the centre of the MBB, surrounded by six Zn1 atoms in an exact octahedral coordination environment (Figure S6b). Each of these six Zn1 atoms is further coordinated by four olate oxygen atoms of four imidazolate ligands (two O2 and two O3) and one O4 forming a octahedral coordination geometry (Figure S7). For electroneutrality we must state that 1/3 of O4 is hydroxide and 2/3 is water. Each of the olate oxygen atoms (O2 and O3) is coordinated to two Zn1 centres; in addition O2 is coordinated to the Zn2 atom. The six Zn2 centres are

surrounded by three imidazolate nitrogen atoms: N1, N2, N6, and three oxygen atoms: O5, O8 of amide moieties and O2 (olate oxygen atom) to form a twofold face-capped tetrahedron (Figure S7). Both Zn3 atoms are coordinated by six nitrogen atoms from three imidazolate nitrogen atoms (N5 and symmetry related atoms) and three amide nitrogen atoms N7 in a distorted trigonal prismatic fashion (Figure S7).

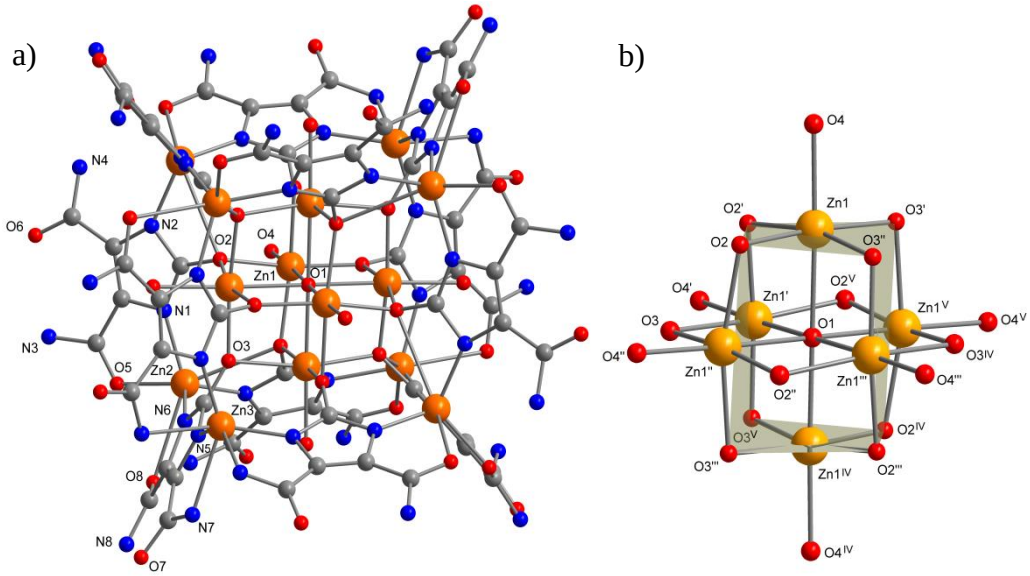

Figure S6. a) Tetradecanuclear zinc the MBB with the three zinc centres (Zn1, Zn2 and Zn3) of **1**, for symmetry operators see legend of Table S4; b) central core of MBB (hydrogen atoms were omitted for clarity; for symmetry code - see legend of Table S4).

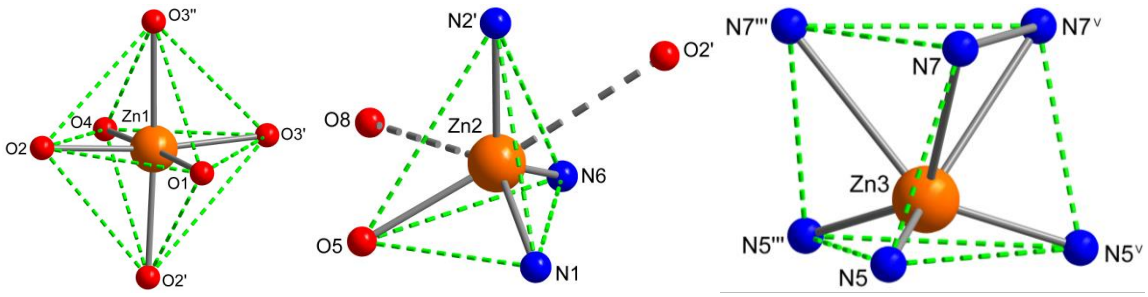

Figure S7. The three zinc centres (Zn1, Zn2 and Zn3) of **1** in the MBB, for symmetry operators see legend of Table S4.

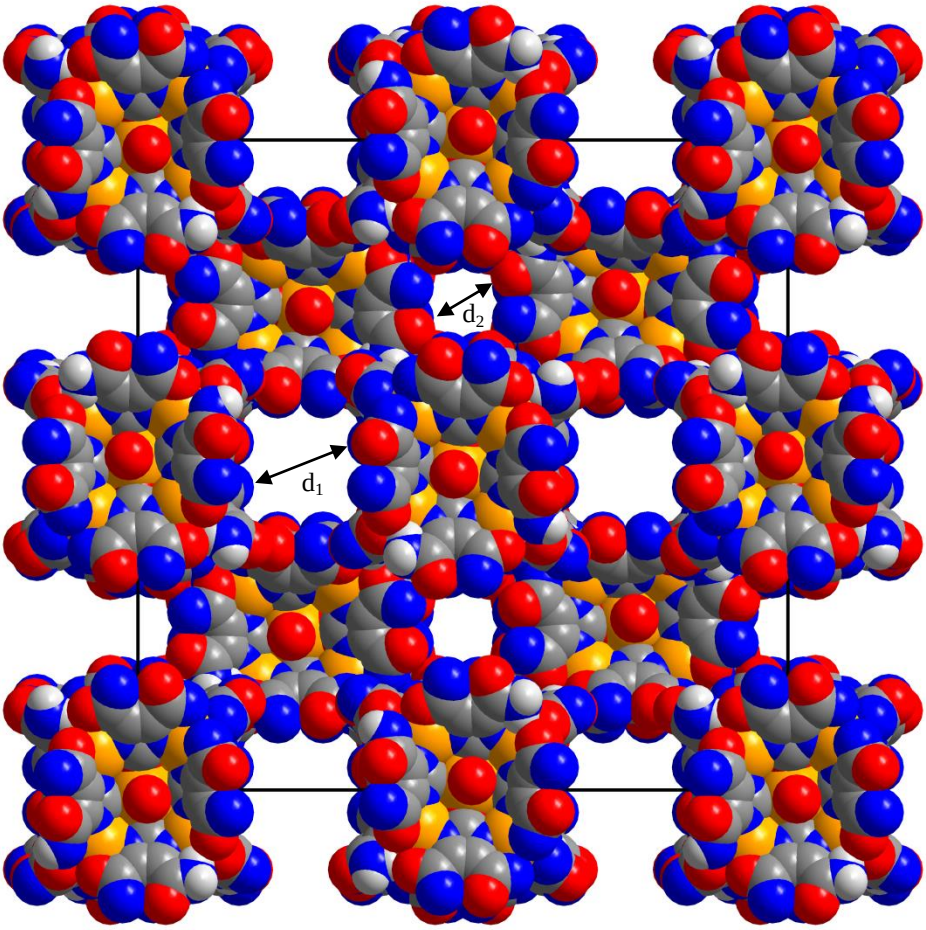

Figure S8. Space filling model for **1**, having two types of channels (approximate diameter, d_1 = 6.0 Å and d_2 = 3.9 Å, orange Zn, blue N, red O, dark gray C, light gray H).

Table S2. Donor-Acceptor distances of the hydrogen -bonds [Å] for **1**.

	D···A
N3 - H3A···O6	2.664(9)
N8 - H8B···O7	2.74(2)
N3 - H3B···O6^{VII}	2.790(9)
N4 - H4A···O5^{II}	3.26(1)
N4 - H4A···O8^{II}	2.87(1)
N4 - H4B···O5^{VI}	3.006(8)
N4 - H4B···O8^{VI}	3.21(1)

Symmetry codes - see legend of Table S4.

Table S3. Selected bond lengths [Å] for **1**.

Zn1 - O1^{II}	2.1914(7)
Zn1 - O2	2.027(4)
Zn1 - O3^{II}	1.986(5)
Zn1 - O4	2.094(6)
Zn2 - O5	2.081(4)
Zn2 - N1	2.013(5)
Zn2 - N2^{I}	1.996(5)
Zn2 - N6	1.968(5)
Zn3 - N5^{III}	1.981(5)
Zn3 - N7^{V}	2.512(1)

Zn2···O2^{I}: 2.819(7) Å; Zn2···O8: 2.730(7) Å

Table S4. Selected bond angles [°] for **1**.

Zn1 - O1 - Zn1^{II}	180.00(4)
Zn1 - O1 - Zn1^{II}	89.72(3)
O3 - Zn1 - O2^{I}	171.0(2)
O3 - Zn1 - O4^{I}	92.1(2)
O2 - Zn1 - O4	92.6(2)
O3 - Zn1 - O1^{I}	89.20(1)
O2 - Zn1 - O1	86.4(1)
O4 - Zn1 - O1	177.65(2)
N6 - Zn2 - N2^{I}	115.2(2)
N6 - Zn2 - N1	114.7(2)
N2 - Zn2 - N1^{I}	113.0(2)
N6 - Zn2 - O5	115.4(2)
N2 - Zn2 - O5^{I}	114.8(2)
N1 - Zn2 - O5	78.83(2)
N5 - Zn3 - N5^{III}	111.40(1)
N5 - Zn3 - N7^{III}	69.6(3)
N7 - Zn3 - N7^{III}	72.4(5)

Symmetry Operators: ^{I}0.5-z,0.5+x,y-1 ^{II}-0.5+y,1+z,0.5-x ^{III}0.5+z,1.5-x,1-y ^{IV}1-x,2-y,-z ^{V}1.5-y,1-z,x-0.5 ^{VI}0.75–x,1.25-z,-0.75+y ^{VII}0.75-x,0.75+z,1.25-y

8 Topological Analysis

Topological Analysis by TOPOS program
##################################
1:zn1
##################################

Structure consists of molecules (ZD1). The composition of molecule is C60H58N48O43Zn14
Topology for ZD1

Atom ZD1 links by bridge ligands and has
Common face with R(A-A) f Total SA

ZD 1	0.2500	0.2500	0.2500	(0-1 0)	17.402A	6	13.89
ZD 1	0.2500	-0.2500	0.2500	(0 0 0)	17.402A	6	13.89
ZD 1	0.2500	-0.2500	-0.2500	(0 0-1)	17.402A	6	13.89
ZD 1	0.7500	-0.2500	-0.2500	(0-1-1)	17.402A	6	13.89
ZD 1	0.7500	0.2500	-0.2500	(0 0-1)	17.402A	6	13.89
ZD 1	0.7500	0.2500	0.2500	(1 0 0)	17.402A	6	13.89
ZD 1	0.2500	0.2500	-0.2500	(0 0 0)	17.402A	3	8.33
ZD 1	0.7500	-0.2500	0.2500	(0-1 0)	17.402A	3	8.33

Structural group analysis

Structural group No 1

Structure consists of 3D framework with ZD

Coordination sequences

ZD1: 1 2 3 4 5 6 7 8 9 10
Num 8 26 56 98 152 218 296 386 488 602
Cum 9 35 91 189 341 559 855 1241 1729 2331

TD10=2331

Vertex symbols for selected sublattice

ZD1 Point symbol:{4^24.6^4}
Extended point
symbol:[4.4.4.4.4.4.4.4.4.4.4.4.4(3).4(3).4(3).4(3).4(3).4(3).4(3).4(3).4(3).4(3).4(3).4(3).4(3).6(18)
.6(18).6(18).6(18)]

Point symbol for net: {4^24.6^4}
8-c net; uninodal net

Topological type: bcu body centered cubic; 8/4/c1; sqc3 (topos&RCSR.ttd) {4^24.6^4} - VS [4.4.4.4.4.4.4.4.4.4.4.4.4(3).4(3).4(3).4(3).4(3).4(3).4(3).4(3).4(3).4(3).4(3).4(3).4(3).*.*.*.*] (73689 types in 11 databases)

Comparison with other H-bonded Frameworks

The occurence of supramolecular hydrogen-bonded frameworks in crystals of metal complexes with organic ligands has been topologically analyzed by Baburin.[9] Baburin classified 636 hydrogen-bonded frameworks in 674 structures into 78 types of three-dimensional nets. As in other frameworks also in the H-bonded nets the trend to close packed motifs prevails. In the H-bonded nets the node connectivity (node degree) ranges from 3-16.

Node degrees of 8 as in the Zn_{14} network **1** encompass 184 out of the 636 analyzed frameworks and follow in abundance after the H-bonded networks with node degrees of 6 with 253 cases. Hydrogen-bonded molecular metal-organic frameworks with node degrees of 8 can be of 17 different types, including bcu, hex, tsi, thp, eci, vcs etc.

The majority of networks with a node degree of 8, that is 79 out of 184, belong to the body-centered cubic, bcu type, as does the Zn_{14} network **1**. After the primitive cubic, pcu type for node degrees of 6 with 210 occurrences, the bcu type for node degrees of 8 is the most abundant one with 79 entries.

The most frequent space groups for the 79 bcu nets were $P2_1/c$ (62.2%), *Pbca* (11.0%) and *Aba2* (3.7%). The maximal space-group symmetry for the 8-nodal degree bcu net is given by Baburin as *Im–3m* belonging to the Laue class 4/*m* –3 2/*m* and point group *m* –3 *m* as does the space group *Ia*–3*d* for the Zn_{14} network **1**.

Various molecular building blocks (MBBs) with metal-organic cubes (MOCs)[10] (Figure S9a) or metal-organic squares (MOSs)[11] (Figure S9b) can be designed and programmed to contain complementary peripheral functional groups. In most cases the linkers such as 4,5-imidazoledicarboxylic acid (Figure S9a), 1,2,3-triazole-4,5-dicarboxylic acid and 2,5-pyridinedicarboxylic acid and other polytopic multidentate linkers are pre–designed. The linkers are used as bridging linkers because of their unique potential to offer peripheral uncoordinated oxygen centres when chelated to a metal ion in N,O-bis(monodentate) fashion, leading to tetra, octa or dodecanuclear cluster nodes. Moreover, diamines were employed as capping ligands because they introduced additional hydrogen-bonding sites on the periphery of the molecular squares (Figure S9b), which are necessary for predictable N–H···O hydrogen bonds to form the frameworks. However, in compound **1** the linker was not pre-designed and formed by *in situ* hydrolyzation of the cyano groups into amide groups. Normally, the linker

is to fully hydrolyzed to carboxylate group under such condition. Additionally, *in situ* hydrolysis of the methoxy to the hydroxy group allows the linker to chelate the metal ion by locking it into its position through the formation for Zn14 metal nodes, compared with others carboxylate based linkers. Moreover, no capping ligand was added to the reaction mixture because free amides of MBB which are directed to vertices are involved with other MBBs via hydrogen-bonds. Different types of nets of various clusters are presented in Table S5.

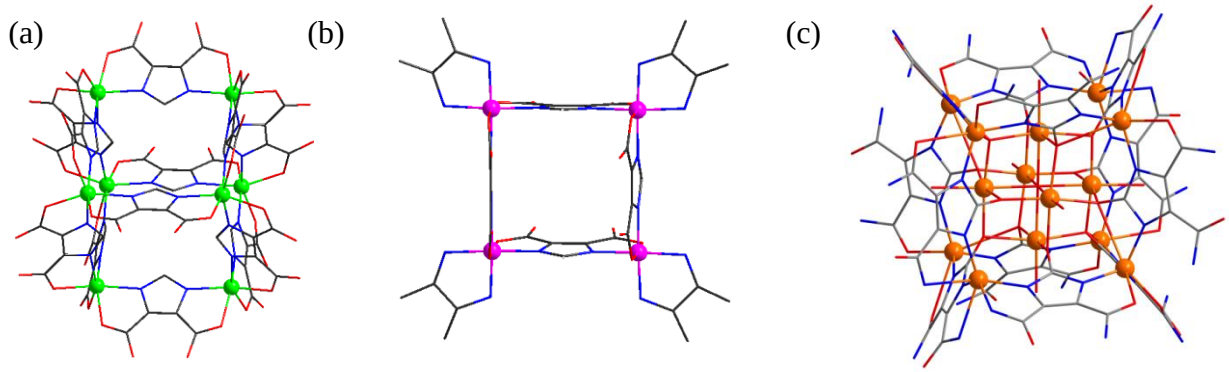

Figure S9. Schematic presentations of (a) In_8 nodes based metal organic cube (MOC)[10a] (b) Co_4 nodes based metal organic square (MOS),[11] formed from 4,5-imidazoledicarboxylate linkers. Each building block is connected through its vertices or edges with other building blocks by intermolecular O–H···O hydrogen bonds, generating supramolecular assembly, (c) tetradecanuclear zinc MBB for **1**.

Table S5. Comparison of various nodes of different cluster based networks.

Serial No.	Linker name	Nodes	Topology/ nets	Reference
1	imidazolate-4,5-diamide-2-olate	Zn_{14}	bcu	this study
2	4,5-imidazoledicarboxylic acid	In_8	zeolite ACO	*J. Am. Chem. Soc.* **2009**, *131*, 10394.
3	4,5-imidazoledicarboxylic acid	In_8	zeolite AST	*J. Am. Chem. Soc.* **2009**, *131*, 10394.
4	4,5-imidazoledicarboxylic acid	Co_4	zeolite gis	*J. Am. Chem. Soc.* **2010**, *132*, 18038.
5	1,2,3-triazole-4,5-dicarboxylic acid	In_4	zeolite rho	*J. Am. Chem. Soc.* **2010**, *132*, 18038.
6	4,5-imidazoledicarboxylic acid	Zn_8	zeolite AST	*J. Am. Chem. Soc.* **2009**, *131*, 17753.
7	4,5-imidazoledicarboxylic acid	Cd_8	zeolite LTA	*J. Am. Chem. Soc.* **2009**, *131*, 17753.
8	4,6-pyrimidicarboxylate	InN_4	sodalite topology	*J. Am. Chem. Soc.* **2008**, *130*, 3768.
9	2-pyrimidinecarboxylate	CdN_4	rho zeolite net	*J. Am. Chem. Soc.* **2008**, *130*, 3768.
10	4,5-imidazoledicarboxylic acid	InN4	zeolite rho topology	*Chem. Commun.* **2006**, 1488.
11	5-tetrazolylisophthalic acid	Cu_{12}	(3,24)-connected rht net	*J. Am. Chem. Soc.* **2008**, *130*, 1833.
12	3,5-dicarboxyl-(3',5'-dicarboxylazophenyl) benzene	Ni	12-connected fcu net10	*J. Am. Chem. Soc.* **2008**, *130*, 1560.
13	H4BIPA-TC	Co	NbO -like	*J. Am. Chem. Soc.* **2008**, *130*, 1560.
14	1H-imidazole-4,5-dicarboxlylic acid	Cd_4	$4\cdot8^2$fes	*Cryst. Growth Des.* **2012**, *12*, 1697.
15	2,5-pyridinedicarboxylic acids	4-connected node, *cis*-$InN_2(CO_2)_2$	Kagomé lattice topology	*J. Am. Chem. Soc.* **2005**, *127*, 7266.

9 Thermogravimetric (TG) analysis

The TG measurements were performed in a stationary air atmosphere (no purge) from room temperature up to 900 °C using a Linseis thermal analyzer (Linseis, Germany) working in vertical mode. The heating rate was 10 °C/min. The samples were placed in cups of aluminium oxide.

The as-synthesized sample of **1** exhibited a continuous weight loss upon heating. Activated sample showed weight loss of 2.8 % (calculated for loss of 4 H_2O 2.3 %) at 25–105 °C, corresponding to the release of coordinated water molecules (aqua ligands). No stable plateau was observed.

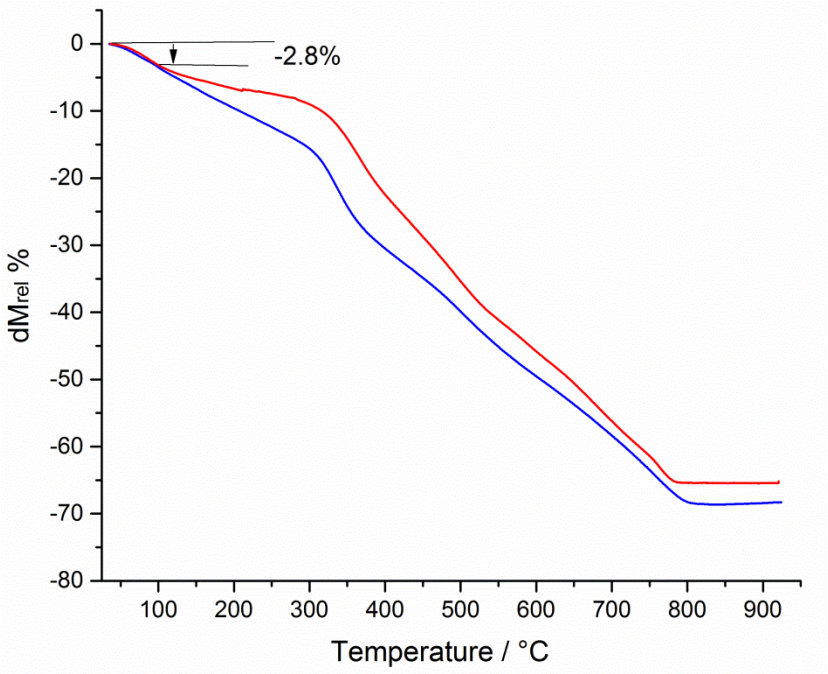

Figure S10. TGA curves for **1** (color: blue = as-synthesized, red = activated).

10 Chemical Stability

Material is stable at ambient air and moisture. Moreover, the chemical stability of the material was analyzed by suspending the samples for 2 days in boiling methanol and water. After such extensive treatment, the material is irreversibly transformed to a so-far unknown crystalline phase (Figure S11). Hence, it can be concluded that the non-rigid H-bonded framework is solvothermally unstable above 65 °C.

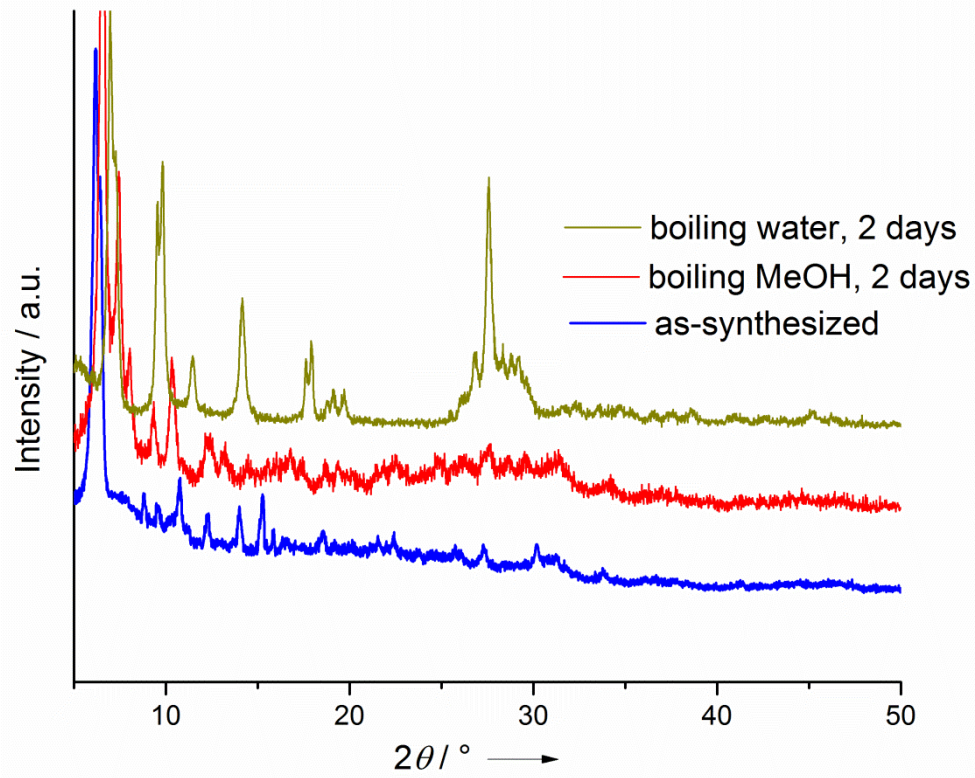

Figure S11. Powder X-ray diffraction profiles of **1** collected during the chemical stability tests in refluxing methanol and water.

10 Gas-sorption measurements

The sample was connected to the preparation port of the sorption analyzer and degassed under vacuum until the out gassing rate, i.e., the rate of pressure rise in the temporarily closed manifold with the connected sample tube, was less than 2 μTorr/min at the specified temperature 50 °C for 24 h. After weighing, the sample tube was then transferred to the analysis port of the sorption analyzer. All used gases (H_2, He, N_2, CO_2, CH_4) were of ultra high purity (UHP, grade 5.0, 99.999%) and the STP volumes are given according to the NIST standards (293.15 K, 101.325 kPa). Helium gas was used for the determination of the cold and warm free space of the sample tubes. H_2 and N_2 sorption isotherms were measured at 77 K (liquid nitrogen bath), whereas CO_2 and CH_4 sorption isotherms were measured at 298±1 K (passive thermostating) and 273.15 K (ice/deionized water bath).The heat of adsorption values and the DFT calculations ('N_2 DFT slit pore' model) were done using the ASAP 2020 v3.05 software.

Table S6. N_2 uptake at 77 K and 1 bar for three consecutive runs on the same probe.

	S_{BET} [m^2g^{-1}]	$S_{Langmuir}$ [m^2g^{-1}]
1st run	465	565
2nd run	471	570
3rd run	468	567

The hydrogen-bonding interactions at **1** can be ruptured to some extent upon activation, giving even smaller particles or cracks in the crystals. Moreover, PXRD pattern of activated sample showed slight broad peaks. Therefore, we repeated the N_2 sorption measurement two times on the same sample and confirmed the reproducibility of the results (Table S6). Hence, we confirmed that non-rigid H-bonded framework is still active for gas-sorption under such activated condition.

Table S7. Comparison of characteristic sorption data of **1** with selected azolate-based hydrogen-bonded supramolecular frameworks (MOC-3 and ZSA-2), hydrogen-bonded porous organic compounds (SOF-1a, HOF-1a, CBDU and TTEB) and ZIFs.

	SA_{BET} [m^2g^{-1}]	$SA_{Langmuir}$ [m^2g^{-1}]	V (N_2) [cm^3g^{-1}]	V (CO_2) [cm^3g^{-1}]	wt % (H_2)	Ref.
1	**471**[a]	**570**[a]	**172**[b]	**56**[c]/**38**[d]	**0.85**[b]	this study
MOC-3	–[e]	456	165[f]	–[d]	0.75[f]	*J. Am. Chem. Soc.* **2009**, *131*, 10394.
ZSA-2	395	–[e]	120[f]	–[e]	0.35[g] / 0.95[h]	*J. Am. Chem. Soc.* **2010**, *132*, 18038.
SOF-1a	474[i]	639[i]	143[i]	16[d]	–[e]	*J. Am. Chem. Soc.* **2010**, *132*, 14457.
HOF-1a	359[j,k]	609[k]	–[e]	225[l]	–[e]	*J. Am. Chem. Soc.* **2011**, *133*, 14570.
CBDU	341[j]	–[e]	–[e]	72[m]	–[e]	*Chem. Mater.* **2006**, *18*, 4855.
TTEB	278[a]	–[e]	–[e]	–[e]	3.9[n]	*Angew. Chem. Int. Ed.* **2009**, *48*, 3273.
TTP	–[d]	240[a]	–[d]	22[d]	–	*Angew. Chem. Int. Ed.* **2005**, *44*, 1816; *Microporous Mesoporous Mater.* **2006**, *88*, 170.
ZIF-95	1050	–	–	19.7[d]	–	*Nature* **2008**, *453*, 207; *Acc. Chem. Res.* **2010**, *43*, 58.
ZIF-100	595	–	–	32.6[c]	–	*Nature* **2008**, *453*, 207; *Acc. Chem. Res.* **2010**, *43*, 58.
ZIF-81	760	–	–	38.2[d]	–	*J. Am. Chem. Soc.* **2009**, *131*, 3875.
ZIF-79	810	–	–	33.5[d]	–	*J. Am. Chem. Soc.* **2009**, *131*, 3875.
ZIF-69	950	–	–	40.6[d]	–	*J. Am. Chem. Soc.* **2009**, *131*, 3875.
ZIF-68	1090	–	–	37.6[d]	–	*J. Am. Chem. Soc.* **2009**, *131*, 3875.

[a] Determined by N_2 sorption at 77 K with data points in the range for p/p_0 between 0.01 and 0.05 for determining BET surface area and between 0.01 and 0.15 for the Langmuir surface area. [b] Measured at 77 K and $p/p_0 \approx 0.97$. [c] Measured at 273 K and 1 bar. [d] Measured at 298 K and 1 bar. [e] Not reported. [f] Approx. value was taken from SI. [g] Measured at 298 K and 80 bar. [h] Measured at 77 K and 20 bar. [i] Calculated from N_2 adsorption at 125 K and 1 bar. [j] Determined by CO_2 adsorption at 196 K. [k] Data points p/p_0 between 0.1 and 0.3 and BET C-constant is negative. [l] At 196 K and 1 bar. [m] 196 K, 1 bar at $p/p_0 = 0.5$. [n] At 77 K and 10 bar.

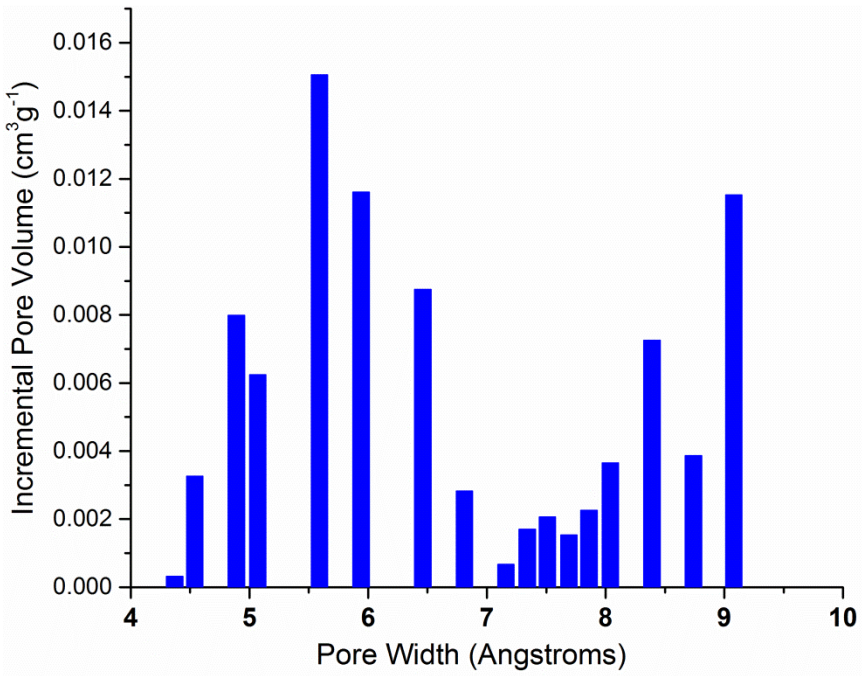

Figure S12. The pore size distribution from a CO_2 adsorption isotherm at 273 K, calculated by the NL-DFT with a "CO_2 on carbon based slit-pore" model at 273 K.

Heat of adsorption

From two adsorption isotherms acquired at different temperatures T_1 and T_2, the differential heat of adsorption $\Delta H_{ads,diff}$, that is isosteric heat of adsorption Q_{st} can be calculated for any amount of adsorbed substance after determining the required relative pressures p_1 and p_2. A modified form of the Clausius-Clapeyron equation is used (eq (1))[12] $\Delta H_{ads,diff}$ was calculated over the whole adsorption range from the 273 K and 298 K isotherms for CO_2.

$$\Delta H_{ads,diff} = Q_{st} = -Rln\left(\frac{p_2}{p_1}\right)\frac{T_1T_2}{T_2-T_1} \qquad (1)$$

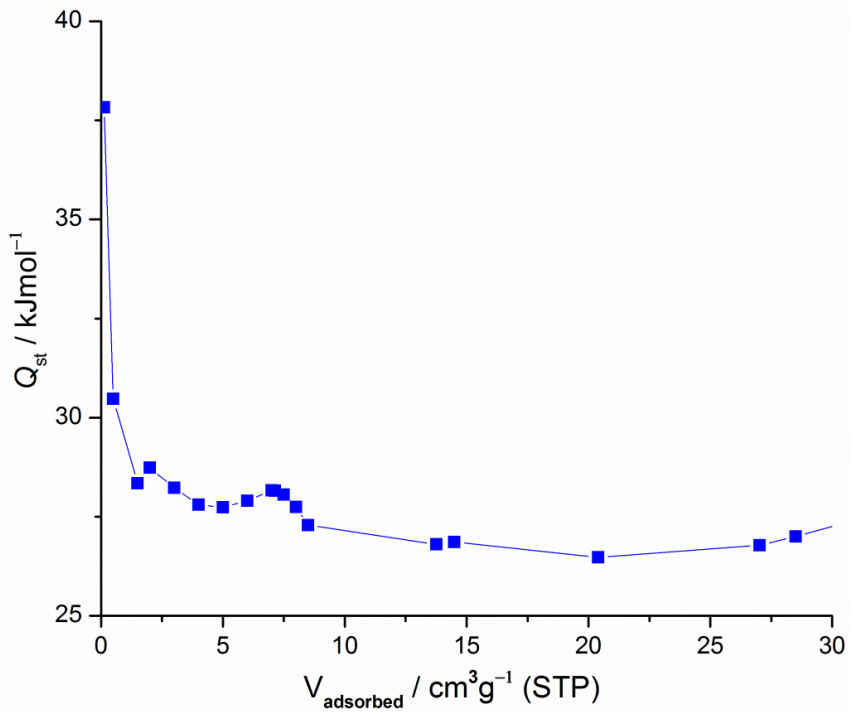

Figure S13. Isosteric heats of CO_2 adsorption as a function of the adsorbent loading for **1**.

12 References

[1] Anderson, W. K.; Bhattacharjee, D.; Houston, D. M. *J. Med. Chem*. **1989**, *32*, 119–127.

[2] Mondal, S. S.; Bhunia, A.; Baburin, I. A.; Jäger, C.; Kelling, A.; Schilde, U.; Seifert, G.; Janiak, C.; Holdt, H.-J. *Chem. Commun.* **2013**, *49*, 7599–7601.

[3] Keene, T. D.; Price, D. J.; Kepert, C. J. *Dalton Trans*. **2011**, *40*, 7122–7126.

[4] Gottlieb, H. E.; Kotlyar, V.; Nudelman, A. *J. Org. Chem.* **1997,** *62*, 7512–7515.

[5] Sheldrick, G. M. SHELXS-97 Program for the Crystal Structure Solution, University of Göttingen, Germany, **1997**.

[6] Sheldrick, G. M. SHELXL-2013 Program for the Crystal Solution Refinement, University of Göttingen, Germany, **2013**.

[7] Blatov, V. Nanocluster analysis of intermetallic structures with the program package TOPOS, *Struct. Chem.* **2012**, *23*, 955–963.

[8] Spek, A. L. *PLATON*, Multipurpose Crystallographic Tool, Utrecht University, Utrecht, The Netherlands, **2008**.

[9] Baburin, I. A. *Z. Kristallogr*. **2008**, *223*, 371-381.

[10] (a) Sava, D. F.; Kravtsov, V. Ch.; Eckert, J.; Eubank, J. F.; Nouar, F.; Eddaoudi, M. *J. Am. Chem. Soc.* **2009**, *131*, 10394–10396. (b) Alkordi, M. H.; Brant, J. A.; Wojtas, L.; Kravtsov, V. Ch.; Cairns, A. J.; Eddaoudi, M. *J. Am. Chem. Soc*. **2009,** *131*, 17753–17755.

[11] Wang, S.; Zhao, T.; Li, G.; Wojtas, L.; Huo, Q.; Eddaoudi, M.; Liu, Y. *J. Am. Chem. Soc.* **2010**, *132*, 18038–18041.

[12] Rouquerol, F.; Rouquerol, J.; Sing, K. *Adsorption by powders and porous solids*, (F. Rouquerol, J. Rouquerol, K. Sing, Eds.), Academic Press, San Diego, **1999**, vol. 11.